



# Signals of northward propagating monsoon intraseasonal oscillations (MISOs) in the RegCM4.7 CORDEX-CORE simulation over South Asia domain

Soumik Ghosh<sup>1,2,3</sup> · Arthur J. Miller<sup>1</sup> · Aneesh C. Subramaniam<sup>4</sup> · R. Bhatla<sup>2</sup> · Sushant Das<sup>5,6</sup>

Received: 26 February 2022 / Accepted: 19 February 2023 / Published online: 9 March 2023  
© The Author(s), under exclusive licence to Springer-Verlag GmbH Germany, part of Springer Nature 2023

## Abstract

Northward propagating summer monsoon intraseasonal oscillations (MISOs) in the Indian Ocean region remain poorly understood and difficult to predict. Here we examine a free-running high-resolution regional atmospheric model (RegCM4.7 with 25 km resolution), forced distantly at the boundaries by atmospheric observations (ERA-Interim, 0.75°) and forced locally by observed sea-surface temperature (SST) over the period 1979–2016, to assess its ability to reproduce key aspects of these MISOs. We find that the model MISO exhibits spatial structures and northward propagation characteristics broadly similar to observed MISO when confining the analysis to the 25–90 day period band. The MISO precipitation anomalies are then shown to be consistent with previously known observed relationships to broad-scale sea-level pressure patterns, Inter-Tropical Convergence Zone (ITCZ) positioning, and changes in the regional Hadley Cell component. The total simulated seasonal (JJAS) rainfall anomalies over India are not significantly correlated with observations, indicating that intrinsic variations in the regional model atmosphere dominate most of the precipitation variability. However, the bandpass-filtered MISO anomalies surprisingly exhibit a significant correlation (0.61) with observations. This suggests that instabilities in the regional broad-scale atmospheric circulation, e.g., linked to the ITCZ position or strength, may be partly controlled by the large-scale atmospheric flows specified at the domain boundaries and/or that specified local SST anomalies may help to guide some fraction of the developing model MISO to follow observations. This result motivates further research on MISO initiation and development using this type of regional atmospheric model.

**Keywords** Monsoon intraseasonal oscillation (MISO) · Indian summer monsoon (ISM) · REGional Climate Model v4.7 (RegCM4.7) · Northward propagation of monsoon · Extended empirical orthogonal function (EOF)

## 1 Introduction

✉ Soumik Ghosh  
soumik.ghosh@fulbrightmail.org

<sup>1</sup> Scripps Institution of Oceanography, University of California, San Diego, CA, USA

<sup>2</sup> Department of Geophysics, Banaras Hindu University, Varanasi, India

<sup>3</sup> Present Address: Department of Earth and Planetary Sciences, Weizmann Institute of Science, Rehovot, Israel

<sup>4</sup> Atmospheric and Oceanic Sciences, University of Colorado Boulder, Boulder, CO, USA

<sup>5</sup> Earth System Physics Section, The Abdus Salam International Centre for Theoretical Physics, Trieste, Italy

<sup>6</sup> Present Address: Department of Meteorology (MISU), Stockholm University, Stockholm, Sweden

Over the last few decades, the simulation and prediction of summer monsoon intraseasonal oscillations (MISOs) in the Indian Ocean using global climate models has drawn increasing levels of attention (e.g., Abatan et al. 2021). However, the current generation of climate and weather forecasting models remains limited in prediction skill compared to the potential predictability of the MISO events (e.g., Lee et al. 2015). Understanding and predicting MISO, therefore, remain among the central tasks of the climate research community (Vitart 2014; Vitart et al. 2012). The MISO's realistic simulation and accurate prediction are still challenging using the present generation of climate models due to inadequate model physics and parameterization (Fang et al. 2017; Li et al. 2018; Misra et al. 2018). These modeling deficiencies have been addressed using many advanced

modeling strategies (e.g., Li et al. 2022b), which motivate further investigations to improve our understanding of the models' MISO simulation capability in terms of diagnostics and forecasting.

The tropical intraseasonal variability (ISV) in northern summer that propagates from the equatorial Indian Ocean is referred to as the MISO (Fu et al. 2013; Lee et al. 2013), which regulates the ISV of the Indian summer monsoon (ISM) (Annamalai and Slingo 2001). This ISV of the monsoon is strongly associated with fluctuations of the inter-tropical convergence zone (ITCZ). The MISO have various timescales of propagation, including 3–7 day (oscillation of monsoon trough), 10–20 day, and 30–60 day modes of oscillation. The 10–20 day mode exhibits westward propagation, while the 30–60 days mode has a northward, and slightly eastward, propagation from the equatorial Indian Ocean to northern India (Goswami 2005; Fu et al. 2007). Due to the intrinsic monsoon variability and the Madden-Julian Oscillation (MJO) impact on monsoon circulation, the northward propagating MISOs are very complex in nature, even more complicated than the MJO (Lau and Waliser 2011; Webster et al. 1998).

Climate models often fail to simulate the salient features of boreal summer MISO (Acharya et al. 2013; Sabeerali et al. 2013; Abhik et al. 2016) and underestimate the MISO variance over the equatorial Indian and Pacific Ocean (Sabeerali et al. 2013). The model performance is often limited in simulating the northwest-southeast tilted rain band structure (Waliser et al. 2003; Sperber et al. 2013) and the eastward propagating wave response (Sperber and Annamalai 2008). Major deficiencies exist in the model simulated MISO amplitude, spatial structure, propagation, and precipitation-sea surface temperature (SST) relationship that acts as a barrier for extended range prediction beyond two weeks (Abhilash et al. 2014a, b; Vitart 2014) and limits our understanding of them. These deficiencies in the model simulation likely arise due to improper representation of atmospheric mesoscale activity (i.e., convection, air-sea interaction, Kelvin and Rossby deformation scales, etc.). Due to the complex physical interaction between the atmosphere and ocean, the nonlinearities in these fields may also lead to improper representation of these processes in model simulations, which further leads to biases in MISO simulation.

While global climate models are necessarily very limited in horizontal grid resolution, regional climate models can implement higher resolution to attempt to potentially better simulate atmospheric convection and other processes that are important in MISO simulation (e.g., Chen et al. 2018). This study focuses on the performance of the newly released regional climate model version-4.7 (RegCM4.7) with 25 km resolution in capturing the spatial structure of the northward propagating MISO over the South Asian Coordinated Regional Downscaling Experiment (SA-CORDEX) domain

(Gutowski Jr et al 2016). Previous studies with RegCM have evaluated the performance of different versions of RegCM to understand the ISV during the monsoon over India (Bhatla et al. 2016; Shahi et al. 2021; Ghosh et al. 2019, 2022). But a detailed study of the northward propagating MISO behavior is still needed for comparison to other models' abilities. Although uncoupled atmospheric models like RegCM are known to be somewhat inferior to coupled atmosphere-ocean models in simulating the monsoon ISV (Fu et al. 2007; Misra et al. 2018; Li et al. 2022a), there is still much that can be learned from this high-resolution uncoupled approach.

Our objectives here are to (1) identify whether northward propagating MISO develops within this version of RegCM, (2) isolate the spatial patterns of precipitation that are associated with these MISO events, (3) compare the model MISO structure and propagation characteristics to observations, and (4) link MISO evolution in the model to the simulated fields of sea-level pressure, winds, the regional component of the Hadley Cell, and the ITCZ. This study will help climate scientists and model developers better understand this regional model's capabilities and limitations in simulating MISO and thereby guide future studies of MISO with RegCM in both uncoupled and fully coupled modes.

## 2 Model, data, and diagnostics

### 2.1 Model configuration and experimental design

For this study, we use the latest Abdus Salam International Centre for Theoretical Physics regional climate model, RegCM4.7. The model consists of a hydrostatic dynamical core of the mesoscale model (MM5) (Grell et al. 1994) and the terrain follows a sigma vertical coordinate system. The model cells are based on an Arakawa B-grid, where the thermodynamic variables e.g., temperature and humidity are at the grid center, and wind components are at the corners. More information about RegCM is discussed by Elguindi et al. (2013).

The model has multiple physics parameterization options, which can be used by the modeling community for carrying out sensitivity studies over different CORDEX domains (e.g. Giorgi et al. 2012). In the South Asia (SA-CORDEX) domain, the radiation parameterization is the CCM3 radiation scheme as described by Kiehl et al. (1996). We used the mixed-type cumulus schemes, i.e., MIT convection scheme (Emanuel and Živković-Rothman 1999) over the land and Tiedtke scheme (Tiedtke 1989) over the ocean. The ocean flux parameterization scheme follows Zeng et al. (1998). The land surface scheme of the Community Land Model version 4.5 (CLM4.5) (Oleson et al. 2013) and UW boundary layer scheme (Grenier and Bretherton 2001) is used. The

large-scale (or non-convective) precipitation is represented through the Subgrid Explicit Moisture Scheme (SUBEX) scheme (Pal et al. 2000).

The RegCM4.7 model is run at a horizontal resolution of 25 km, which consists of  $429 \times 337$  grid points over the SA-CORDEX domain ( $15^\circ$  S– $45^\circ$  N;  $10^\circ$  E– $130^\circ$  E) as shown in Fig. 1. The model top is set at 50 hPa and has 23 vertical levels, and the domain center is located at  $13^\circ$  N/ $70^\circ$  E. The RegCM4 simulations are forced by the 6-hourly ERA-Interim ( $\sim 0.75^\circ \times 0.75^\circ$ ), hereinafter called EIN75 (Dee et al. 2011). The EIN75 atmospheric fields are specified at the distant lateral domain boundaries, and the EIN75 SST fields are specified at the local oceanic boundary. The topography and land use data are taken from the United States Geological Survey (USGS), available at  $30''$  resolution. The map projection used is the rotated Mercator and the time step to carry out the simulations is 40 s. The model is integrated from 1st January 1979 to 31st December 2016, a period of availability of EIN75 at the time of this study. The resulting RegCM4 simulated atmospheric fields are “free-running” in the interior domain with no data assimilation.

## 2.2 Observational data

Model precipitation data is validated with the  $0.25 \times 0.25^\circ$  gridded daily precipitation of the Tropical Rainfall Measuring Mission (TRMM). This dataset was only available for the 1998–2016 time period (Huffman and Bolvin 2018) so that forms the time period for direct model comparison with rainfall observations.

## 2.3 Diagnostic approaches and tools

Daily rainfall anomalies from the model and observations are analyzed in various ways for the months of June–September (JJAS) over the entire region. The seasonal average rainfall pattern is first compared as an indicator of the quality of the simulation. Model-observation comparisons of daily rainfall statistics are further quantified with probability density function (PDF) and scatter bin distributions with estimates of the 95% confidence level. For comparison with previous studies of MISO and ISV, four subregions are defined in this analysis and indicated in Fig. 1. These are the Indian subcontinent (land only), Indian Ocean (IO:  $60^\circ$  E– $110^\circ$  E and  $15^\circ$  S– $5^\circ$  N), Bay of Bengal (BoB:  $83^\circ$  E– $93^\circ$  E and  $8^\circ$  N– $22^\circ$  N) and the MISO region ( $55^\circ$  E– $95^\circ$  E and  $15^\circ$  S– $30^\circ$  N). These regions can potentially exert a large impact on monsoon propagation over the Indian subcontinent.

### 2.3.1 Time scales of MISO

Previous studies found that the MISO periodicity lies between 25 and 90 days with an average oscillation of 30 days (e.g. Suhas et al. 2013). We considered only precipitation as our metric of isolating the 25–90 day MISO responsible for part of the ISV (active and break spells) of the Indian summer monsoon (Ghosh 2020). The daily rainfall anomalies (computed by removing the seasonal climatology) were filtered using a 25–90 day bandpass Lanczos filter (in Matlab) to minimize the responses from MISO in the 3–7 day and 10–20 day spectral ranges. All subsequent MISO analyses were performed on these bandpass-filtered fields.

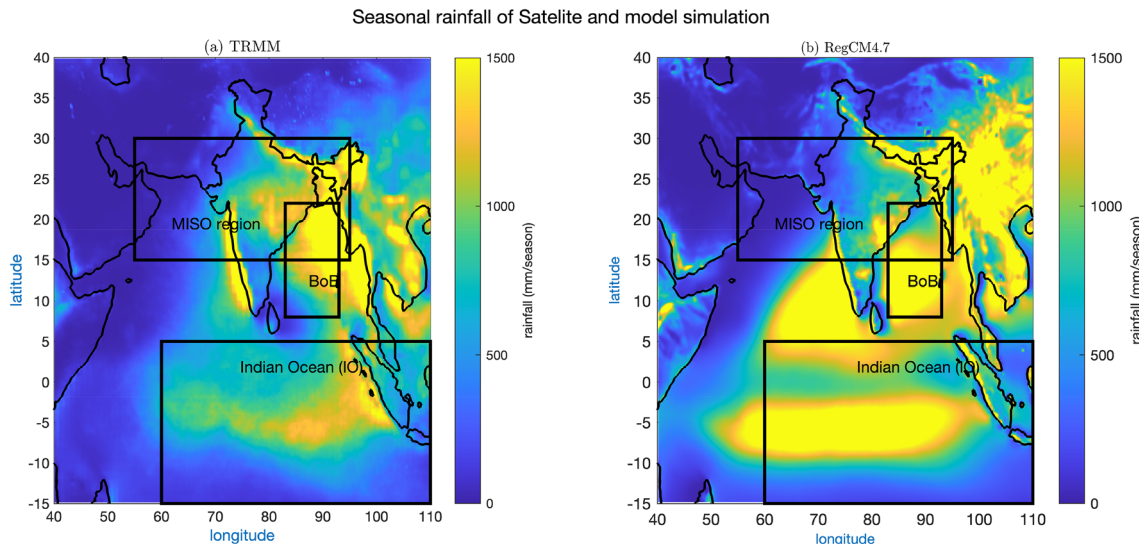


**Fig. 1** Model domain, showing lateral boundaries and continental outline, with defined subregions delineated as black rectangles. The shaded color indicates JJAS seasonal average rainfall of **a** TRMM and

**b** RegCM4.7 simulation. The TRMM rainfall data cover 1998–2016 while the model simulated rainfall includes the entire 1979–2016 simulation

### 2.3.2 Propagation of MISO

We use two approaches to identify northward propagating MISO in the model. The first is by composite analysis based on identifying the occurrences of active rainfall and break periods over India. These provide temporal tags for subsequently forming time-lagged composites of rainfall that can show propagation patterns. The active and break phases of the 25–90 day bandpass-filtered rainfall are identified using the normalized (i.e., deviation of the daily rainfall from the climatology mean divided by the standard deviation) rainfall anomaly. The amplitudes with +1 (−1) are termed active (break) monsoon spells.

The second is by using extended empirical orthogonal function (EEOF) analysis on the precipitation fields to identify temporal phase lags in the dominant spatial structures in the simulation. This method was introduced by Weare and Nasstrom (1982) to extract the potential dynamical propagation structures in oscillations by extending standard EOF analysis to include spatial and temporal correlation over several time lags. This strategy was later used by Kikuchi et al. (2012), who explained its potential capability for real-time MISO predictions. The area between 60.5° E–95.5° E and 12.5° S–30.5° N over the MISO region is used in our EEOF analysis for the 25–90 day filtered rainfall during the months of JJAS, with a series of lags from 0 days to 15 days in 1-day increments, from the RegCM4 simulation (1979–2016). Phase diagrams are also computed for key summers using the first two principal components (PCs; PC-1 and PC-2) of the EEOF analyses.

### 2.3.3 Regional component of the Hadley cell

In order to identify linkages of MISO with the larger-scale background flow, we computed the regional component of the Hadley Cell (RCHC) in the model using the zonal mean mass stream function  $\Psi$ . This is derived from model variables over the Indian monsoon region of 70–95° E using:

$$v = \frac{g}{2\pi a \cos \phi} \frac{\partial \Psi}{\partial p}$$

where  $v$  is the meridional wind,  $p$  is the pressure and  $\phi$  is the latitude.  $g$  is gravity. The RCHC is computed first for the seasonal summer climatology (JJAS). Then the changes in the RCHC pattern for break and active periods of the MISO during are computed as deviations from the summer mean.

### 2.3.4 ITCZ

The position and width of the ITCZ are also of interest as potential links to explaining aspects of MISO behavior.

There are a number of ways to identify the ITCZ. In this study, we use the mass-weighted vertical average of the zonal mean mass stream function (Byrne et al. 2018) integrated between 70 and 95° E, which allows us to identify the position and width of the ITCZ over the Indian monsoon region. The ITCZ width is the distance between the northern and southern edges of the region of upward motion. The pressure level between the 300–700 hPa of the zonal mean mass stream function is averaged to perform the mass-weighted vertical average. The metric identifies the southern edge ( $\phi_S$ ), location ( $\phi_{ITCZ}$ ), and northern edge ( $\phi_N$ ) of the ITCZ along with its width (difference between the  $\phi_S$  and  $\phi_N$ ).

## 3 Results and discussion

### 3.1 Seasonal mean rainfall

Before focusing on the propagating aspects of the atmospheric rainfall over the ocean, we discuss the seasonal mean rainfall distribution during the monsoon period in the model domain. Figure 1a, b shows the seasonal (JJAS) accumulated rainfall over the SA-CORDEX region for both observations and the simulated response. During the summer monsoon, the westerly wind carries a huge amount of water to the Indian landmass and the hills of the western Ghat separate the monsoon wind into two parts. One part directly affects the west part of India and the other part flows to the south-east of the Indian region as the monsoon trough forces the wind to change its direction to the BoB. Propagation of monsoon rainfall follows the monsoon trough as it advances to north and central India through the Gangetic plain. The BoB receives a large amount of rainfall during the season. The foothills of the Himalaya play an important role in directing the monsoon's advance to north and central India. These mechanisms are both at play in both the observations and the model. However, Fig. 1 reveals that the model generates a very large bias of heavy rainfall over broad regions of the open ocean in the Arabian Sea, in the BOB, and under the ITCZ in the equatorial ocean. The near-coastal precipitation responses over land, however, east of the Arabian Sea and east of the BoB are more favorably captured by the model in both magnitude and structure, as is the response over Northeast India. The model response over land in Southeast Asia, in contrast, is also biased toward heavy rain.

We quantified the model bias for two major subregions, the Indian Ocean box in Fig. 1 and the Indian subcontinent land area. The observed seasonal mean accumulated rainfall over India is 571 mm and over the IO is 2945 mm, showing that the ocean receives a huge amount of rainfall compared to the Indian landmass during the observed monsoon season. The modeled seasonal mean rainfall over India in the model

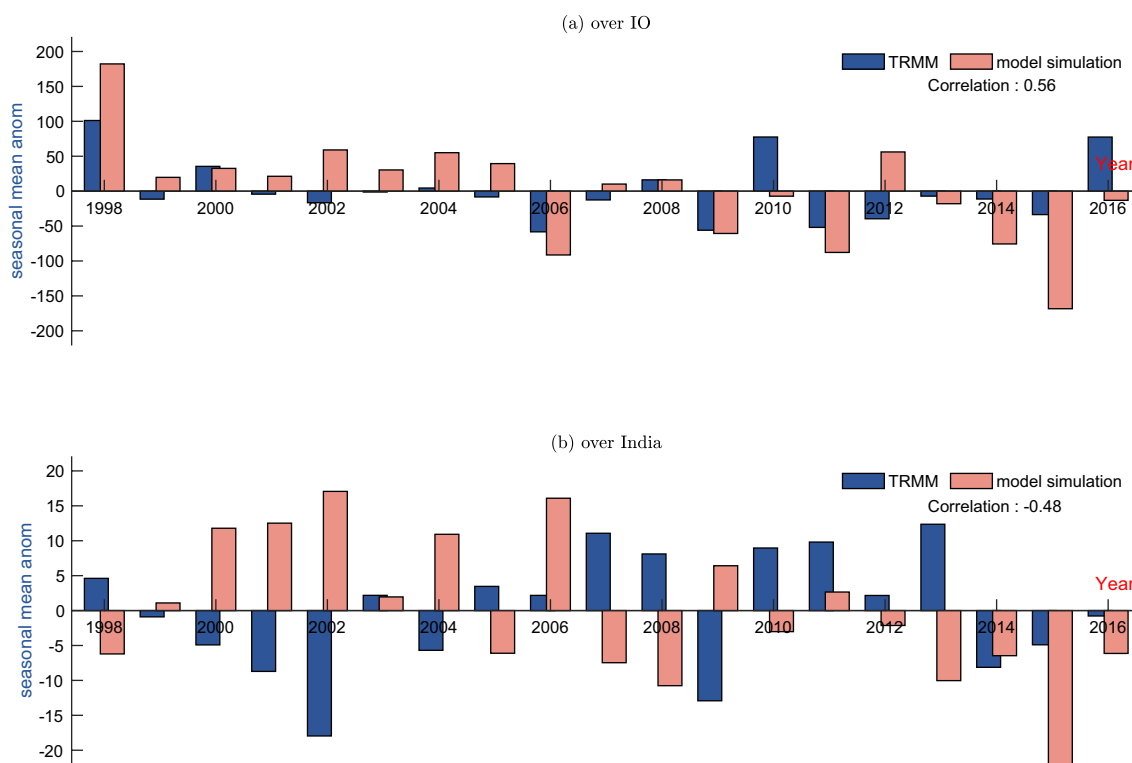


**Fig. 2** Seasonal rainfall anomalies over two important regions **a** Indian subcontinent and **b** Indian Ocean (IO) region for MISO. Note that TRMM was available only from 1998 to 2016, which limits the time period of model-data comparison

is 667 mm, which is significantly higher than the observations, as is the 5153 mm of rainfall over the IO, which is further evidence of the degree of model bias.

The types of strong model precipitation biases seen in Fig. 1 are commonly found in global and regional climate model simulations. While previous work with RegCM (e.g., Ghosh et al. 2022; Agrawal et al. 2021; Maharana and Dimri 2016) has resulted in a steady, though incremental, improvement in the simulation of the monsoon region over time, we are far from properly remedying this precipitation bias problem. However, even with a poorly represented or heavily biased mean state of rainfall, we posit that we can still extract interesting results from studying the propagating components of rainfall that may arise in our modeled system.

### 3.2 Seasonal rainfall anomalies

We next examine the characteristics of the total seasonal (JJAS) rainfall anomalies in the model and observations. Figure 2 shows the rainfall anomalies averaged over two major subregions (the Indian Ocean box in Fig. 1 and over land on the Indian Subcontinent) for both observations and model. Over the tropical Indian Ocean, the model rainfall is significantly correlated (0.56) with the observed, indicating the expected level of thermodynamic control that the specified SST observed anomalies exert on tropical rainfall over

the ocean. But there is no significant positive correlation ( $-0.48$ ) between the model and observations over India for these anomalies, which are the accumulation of all time-scale precipitation variations from daily to seasonal. This result is not surprising since the model is forced at lateral boundaries that are very far away from the development of rainfall events over land in the interior of the model domain. This indicates that intrinsic variations in the regional model atmosphere dominate most of the precipitation variability over land and that boundary conditions and SST anomalies exert minimal control over the seasonally averaged response over land.

### 3.3 Daily rainfall anomalies

The model performance was next evaluated by plotting the statistical distributions of daily rainfall anomalies during the summer monsoon season (JJAS) in four key regions (India, BoB, IO, and MISO, see Fig. 1) for both model and observations in Fig. 3. The data for each region is normalized with their respective standard deviation. To compare the model distribution pattern with observations in different ways, we have used bin scattered matching, PDF, and box plot statistics. The binned scatter is an aggregate statistic that summarizes the bins, which are made by the group of matched data points. This is an informative and versatile way to visualize

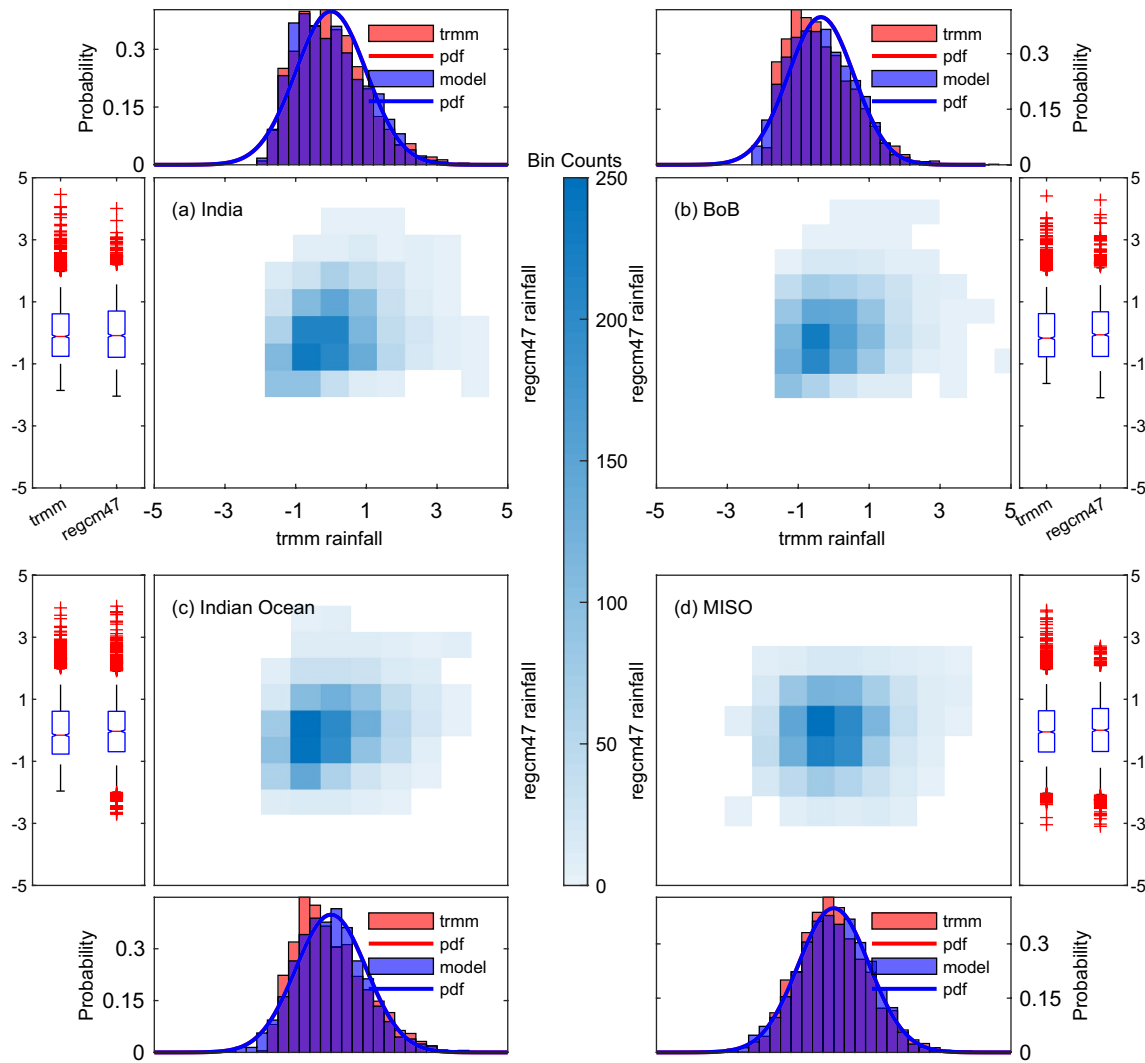


**Fig. 3** Data distributions of observed and modeled daily rainfall over the **a** Indian landmass, **b** Bay of Bengal (BoB), **c** Indian Ocean (IO) and **d** MISO regions. The bin scatter, box plot and PDF distributions are considered for statistical data validation with 95% confidence

the differences in distributions between the variables or between the observed and model simulation. The rectangular shading bins count the density of the matching data points between observation and model simulation. The deep color represents the highly dense bin-occurrence matches between the observations and the model. The PDF is a standardized way to measure the data distribution and a box plot is another common way to display the data distribution by measuring the central tendency (median, mean, and mode) of the data sets. Overall, the modeled and observed distributions seen in Fig. 3 are structurally quite similar in the four regions, although the normalization does not account for differences in magnitude between model and observations. This gives added confidence in our approach to studying the monsoon ISO in this simulation.

level. The data over the respective regions are normalized with their respective standard deviation so that only the structure of the distributions should be compared

### 3.4 Monsoon intraseasonal oscillations (MISOs)

#### 3.4.1 Timescale isolation: 25–90 day bandpass filter

The MISO includes the 10–20 day westward and 25–90 day northward ISO propagation during the summer monsoon season over the MISO region. Along with the difficulties of simulating this behavior, it is a challenge to isolate the northward propagation from the westward propagating components. The first technique we will employ is to attempt to eliminate the higher frequency rainfall (3–7 days) and 10–20 day westward propagating rainfall by bandpass filtering with a 25–90 days Lanczos filter to isolate the northward propagation. Figure 3 shows the 25–90 day band-pass filtered normalized rainfall anomalies for the model and observations

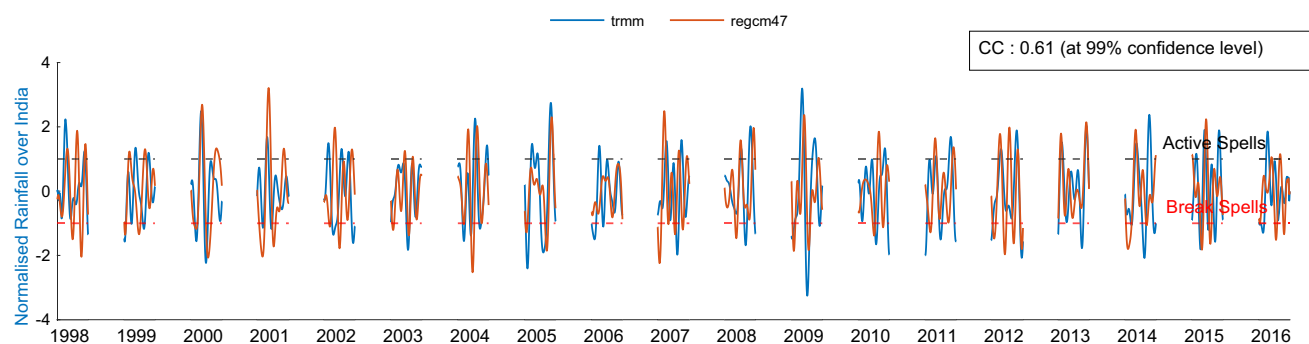


**Fig. 4** Time series of active and break spells over India. The 25–90 days filtered normalized rainfall anomaly over the Indian region is used to identify the active and break spells. The blue line repre-

sents the TRMM rainfall and the red line illustrates the RegCM4.7 simulated rainfall during the summers (JJAS) of the overlapping time period (1998–2016) of observations and model

over India for each summer (JJAS) from 1998–2016, which is the period of overlap of the TRMM observations with the model run. At some times, the model and observations have MISO events that align in phase, while at other times, they do not. The correlation over this time period is significant, 0.61, indicating that approximately 37% of the variance is explained by the model in this period band. This is a surprisingly high correlation since we previously determined that there is little model skill in explaining the seasonal mean rainfall anomalies in this region. This correlation on MISO timescales suggests that instabilities in the regional broad-scale atmospheric circulation, which may initiate MISO events, may be partly controlled by the large-scale atmospheric flows specified at the domain boundaries or by local SST anomalies that may help to guide some fraction of the developing model MISOs to follow observations.

We next consider the MISO periods with enhanced rainfall and the break spells when the rain is reduced. In Fig. 4, the black (red) horizontal lines delineate one standard deviation positive (negative) rainfall MISO anomalies as active (break) days of the monsoon. The model successfully hits 19 peaks of the active spells out of the 34 actual peaks and 19 peaks of the break spells out of the 38 actual breaks. Note that the model also fell short of additional observed peaks/troughs of active/break spells, due to lower model precipitation anomalies that did not exceed the threshold criteria but had the correct phasing. These results suggest that this model is dynamically capable of simulating certain aspects of the MISO response over India, suggesting predictable components that might be exploited in future forecasting efforts.

We next use the active and break MISO periods identified in Fig. 4 to produce regional maps of the MISO structures in these two extreme phases. Figure 5 shows the bandpass filtered rainfall anomalies averaged together at each grid point for each day that they exceed the active/break thresholds for the model and observations. During

the active phase, rainfall anomalies are strongest along the west coast of India, with a broad swath of weaker anomalies extending from central India southeastward across the BoB. A similar negative pattern prevails during the break phase, suggestive of a wavelike response. The model fails to generate a strong rainfall response in western India during the active phase, but it successfully produces rain in central India that extends southeastward into the southwest BoB. The break phase in the model also exhibits an opposite structural response pattern as found in the observations. The model's orientation of the broad swath of MISO rainfall, however, is distorted toward northwest–southeast (clockwise) compared to observations, which are closer to west–east (Ghosh 2020; Shahi et al. 2021), and does not extend strongly into the Andaman Sea like nature. But overall, the model is able to capture a key aspect of the MISO active phases and break spells by exhibiting a broadscale regional response extending from central India across the BoB.

### 3.4.2 Propagation: phase composites and EEOF analysis

We next attempt to identify the propagation of MISO by using the timing of the break phases identified in Fig. 4 to form composites for various time lags. Figure 6 shows composites of the bandpass filtered rainfall anomalies for 3, 6, 9, 12, and 15 days after the peak break phase in Fig. 5c. The lag of 15 days is clearly seen as corresponding to the dominant half-period of MISO (Suhas et al. 2013), since it visually corresponds to the active phase spatial pattern in Fig. 5c. We can also clearly see that the transition of the model MISO from the active phase to the break phase is associated with a northward propagation of the anomalies across the BoB and over India. This northward propagation is further quantified using a Hovmöller diagram in Fig. 7 where rainfall anomalies from Fig. 6 are zonally averaged across India ( $70^{\circ}$  E– $95^{\circ}$  E) and plotted as

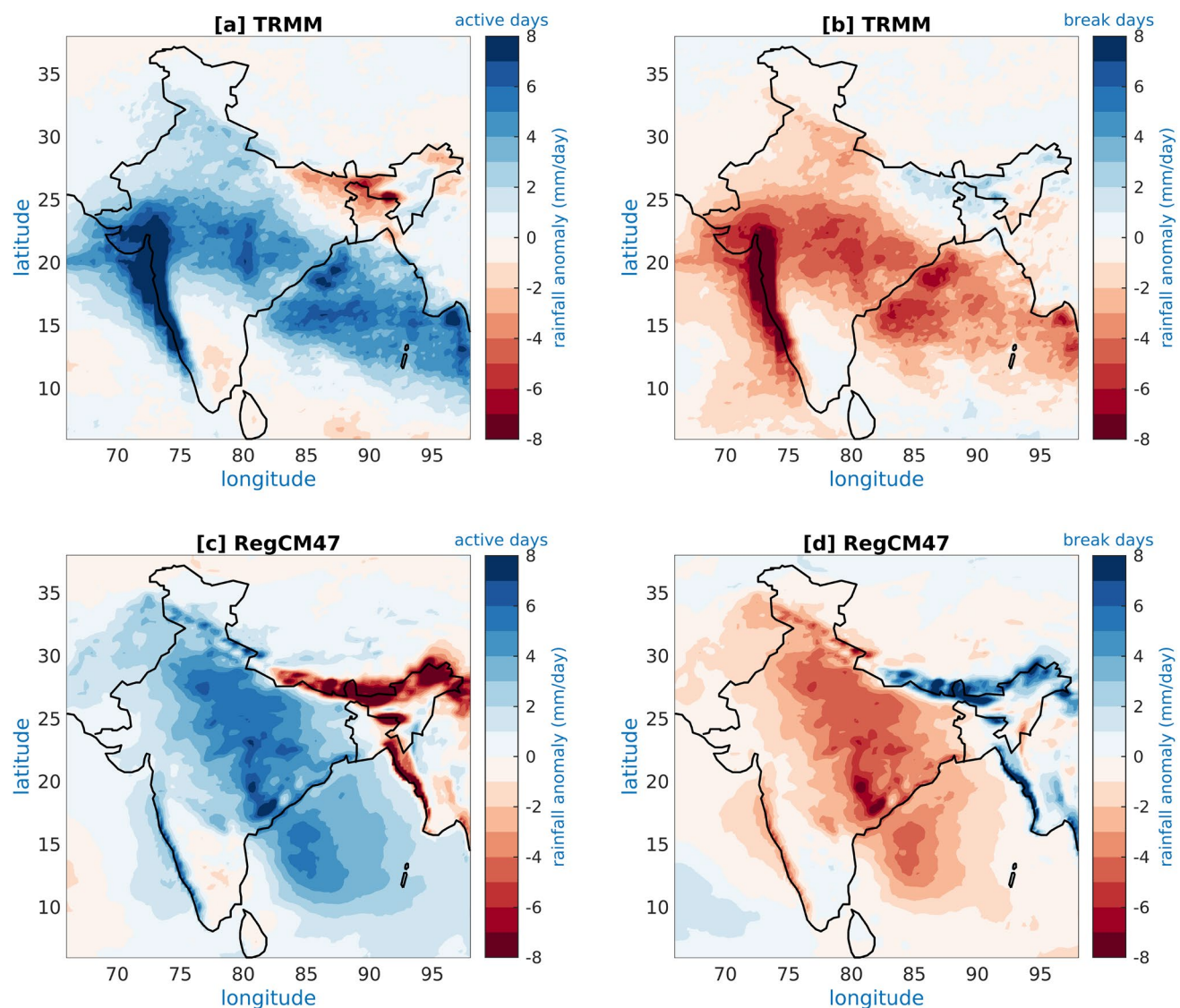


**Fig. 5** Spatial patterns of active and break phases (determined from Fig. 4) of the summer monsoon in TRMM observation (**a**, **b**) and RegCM4.7 simulation (**c**, **d**) using 25–90 days filtered rainfall. The

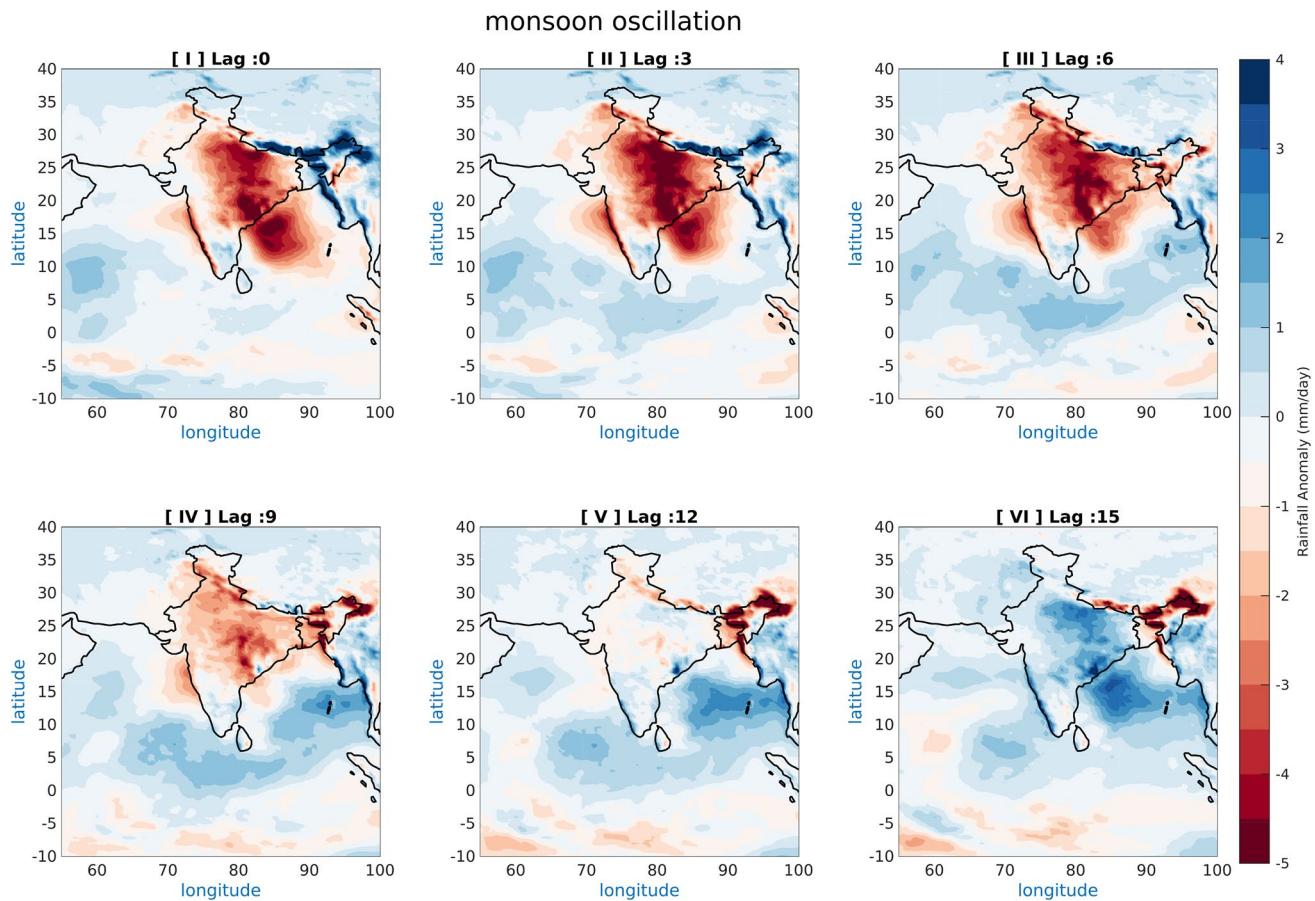
positive anomalies (blue) represent wet conditions (active phase) and the negative anomalies (red) represent the dry conditions (break phase) during the MISO

latitude versus time lag. Although the zero line of the plot is slightly nonlinear, the model MISO propagates approximately  $15^\circ$  latitude over the 15-day lag, yielding a phase speed of  $\sim 1$  deg/day ( $\sim 111$  km/day) that is very similar to observed values during summer (Lau and Waliser 2011; Sikka and Gadgil 1980).

We can further isolate propagating features of the model MISO by applying Extended Empirical Orthogonal Function (EEOF) analysis to the bandpass-filtered model output. For our model output, two modes (EEOF-1 and EEOF-2, which form a spatially and temporally lagged pair) dominate the response and pass the sampling error criterion, while the rest of the modes are considered noise in this context (North et al. 1982). Figure 8 shows the evolution of MISO

EEOF-1 for sequential 3-day lags over 15 days. Note the strong similarity to the composite results shown in Fig. 5. A propagating signal is clearly depicted progressing from Lag-0 to Lag-15 as the active phase moves from the BoB to central India. Lag-6 to Lag-12 cover the transition period from the break phase to the onset of the active phase of the monsoon. The results indicate a 15-day half-period of MISO, which is consistent with the composite analysis result and the 25–90 bandpass filtering, as well as observations (Suhas et al. 2013).

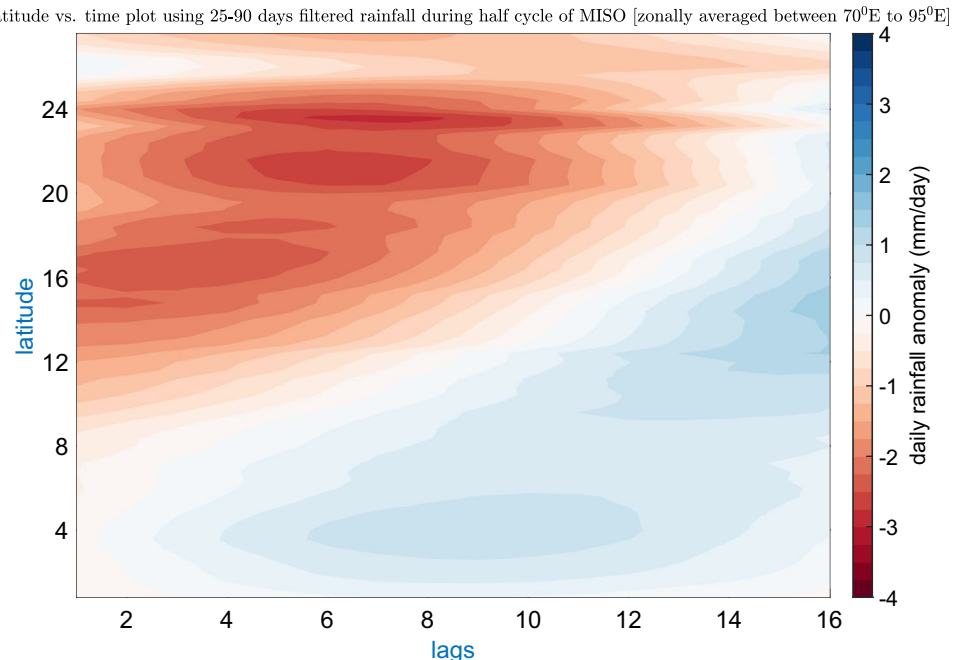
Our final demonstration of the propagating oscillatory behavior of MISO in the model is through phase space diagrams. These are constructed by plotting the two temporal coefficients of the two dominant EEOF modes against each



**Fig. 6** Transition from break to active phase of MISO using 25–90 days model simulated filtered rainfall anomaly (mm/day) for a series of 3-day lag periods after the peak break phase. Here, (I–II) are the break days, (III–IV) are the transition from break days to active days

and (V–VI) are the onset of active days. The phases are identified using the normalized rainfall anomaly matrix over the Indian subcontinent (Fig. 4). Lag-0 is considered as the 0th day and Lag-15 is the 15th day after Lag-0. Lag-0 (I) represents the same plot in Fig. 5d

**Fig. 7** Latitude vs. time Hovmöller diagram of the model simulated 25–90 days filtered rainfall anomalies zonally averaged between 70–95° E showing northward propagation during the 15-day half-period of the model MISO



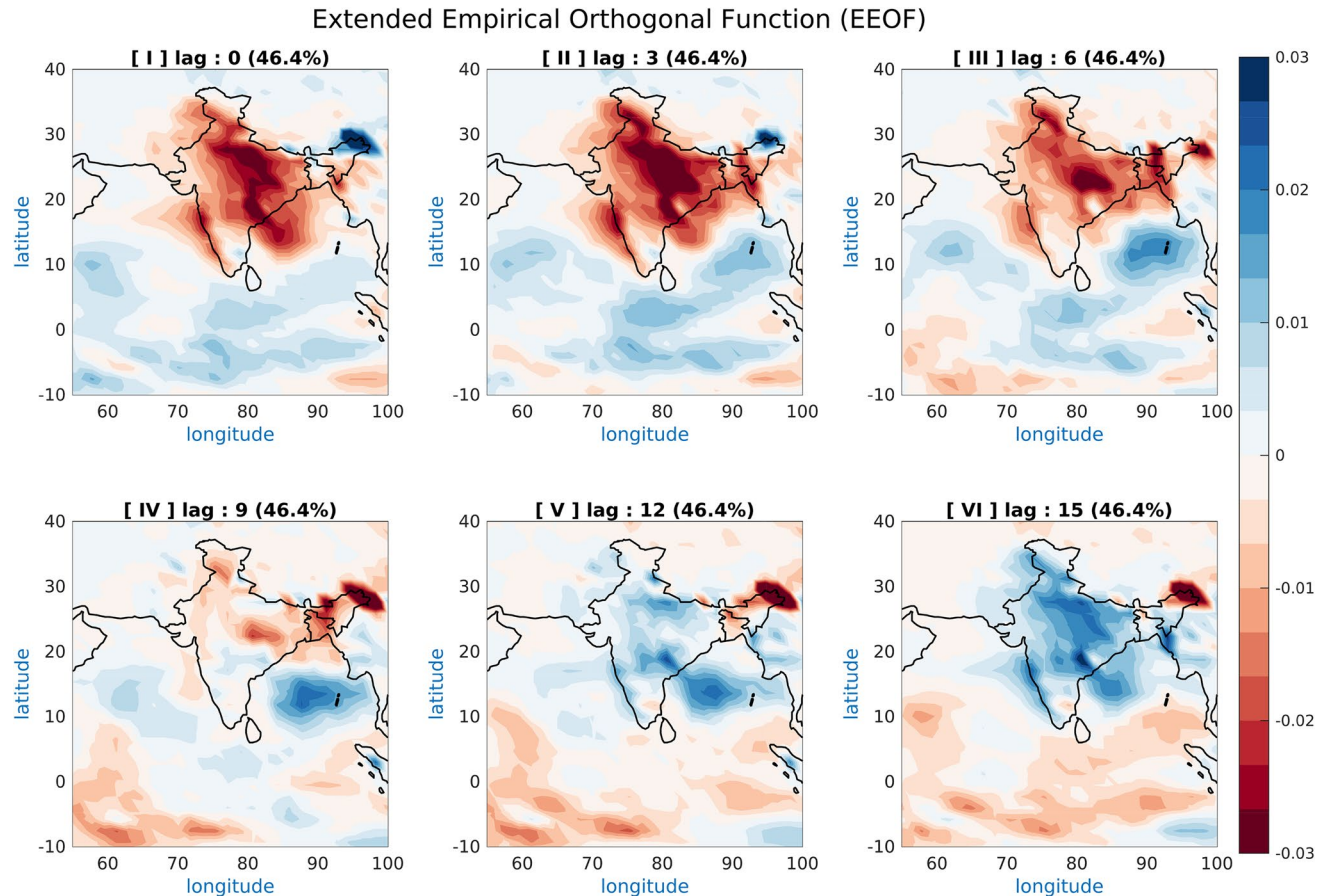


**Fig. 8** Evolution of MISO break phase to MISO active phase using EEOF-1 calculated from 25 to 90 day bandpassed RegCM4.7 simulated rainfall. Here, I–II are the break days, III–IV are the transition from break days to active days and V–VI are the onset of active days

other over time, as seen in Fig. 9. Oscillatory behavior in time is represented by a circular trajectory through eight phases. Oscillatory behavior in space can be associated with the quadrant of the plot that corresponds to the maximum rainfall anomaly location in eight different geographic places (indicated in Fig. 9). Clockwise trajectories indicate northward propagation. Colors indicate the months of the summer. Values of the index that lie outside the unit circle indicate strong MISO activity in the domain. For brevity, we show only four summers, 1991, 1992, 2004 and 2007.

Each year in Fig. 9 exhibits strong MISO activity in the model. In general the MISO signal is stronger in June–July–August, which is when the monsoon advances and peaks, and weaker in September, which is when the monsoon retreats. High-amplitude, clockwise, quasi-circular trajectories are associated with MISO periods of 30–45 days, which is broadly consistent with our previous analyses. The plot also reveals aspects of the strong intermittency in MISO throughout any given summer, but also suggests that predictable MISO components occur in the model, which could be exploited in future forecast studies.

### 3.5 Relationships with other physical variables

#### 3.5.1 Sea level pressure and 850hPa wind

Previous studies Rao (1976) and Mooley and Shukla (1989) have suggested a weak-to-deep low-pressure belt over central India causes weak-to-strong (and prolonged) monsoon periods in observations. The absence of the low-pressure belt over India was suggested to cause breaks in the monsoon. To investigate if this type of relationship holds in the model, we examined the contemporaneous SLP anomalies, along with 850hPa wind anomalies, during the phases of model MISO propagation (Fig. 10i–vi). During the break phases (Lag 0 and Lag 3) high pressure prevails over the northern part of India covering the Gangetic plains and the wind circulates westward across central India. During the transition phases (Lag 6 and Lag 9) strong low pressure develops over central India and expands northward and over the Bay of Bengal (Fig. 10iii–iv). These two lags show how SLP anomalies establish suitable conditions for developing the active monsoon phases in Lags 12 and 15. During Lag 12

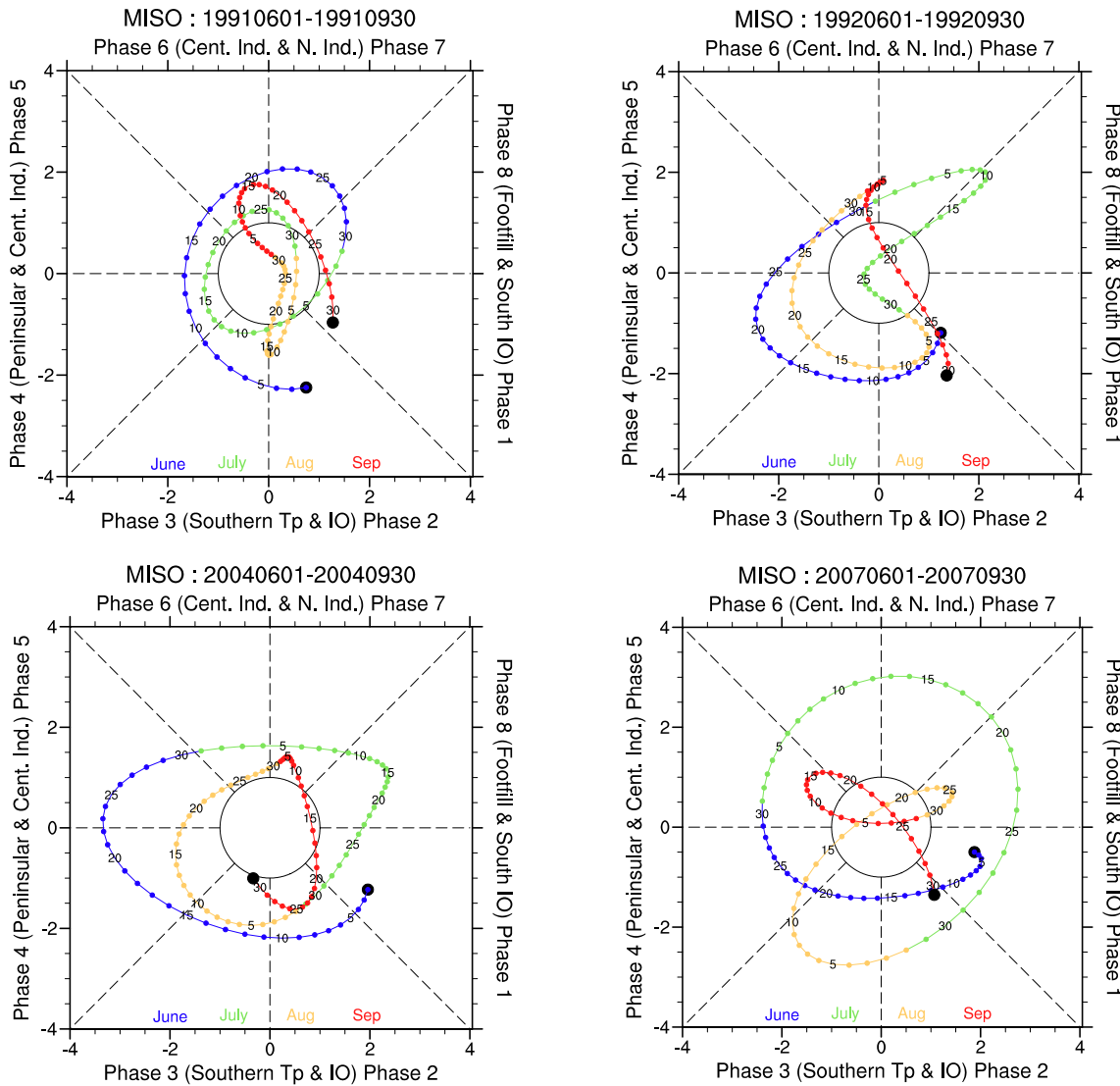


**Fig. 9** Phase space diagram of the RegCM4.7 simulated northward rainfall propagation over the MISO region using EEOF coefficients. The diagram is prepared with the first two principal components (PC-I and PC-II) of the dominant EEOF's for four selected years

the low pressure extends throughout the northern Arabian sea, central India, and the northern BoB (Fig. 10v). This concentrated low-pressure over the northern BoB is important for the advance of the monsoon by its associated winds guiding the high-moisture air from the BoB to central India. During the active phase at Lag 15, the low-pressure belt weakens over India but strengthens over the central BoB and is associated with India experiencing rainfall stretching along a rainband from Northwest India to the central BoB (Figs. 5c, 10vi). These model relations between SLP and precipitation are broadly consistent with the observational analysis discussed by Mooley and Shukla (1989).

### 3.5.2 Regional component of the Hadley cell

We next considered the relation between the model MISO propagation and the regional component of the Hadley Cell (RCHC). The regional meridional overturning mass stream function is used to define the RCHC during the MISO phases to consider its impact. The summer (JJAS) mean RCHC is shown in Fig. 11a. The anomalies from the seasonal mean RCHC during MISO for the break phase (Lag 0) and active phase (Lag 15) are shown in Fig. 11b, c. The anomalies in the RCHC are surprisingly nonlinear in that they do not mirror each other for the break and active phases. During the break

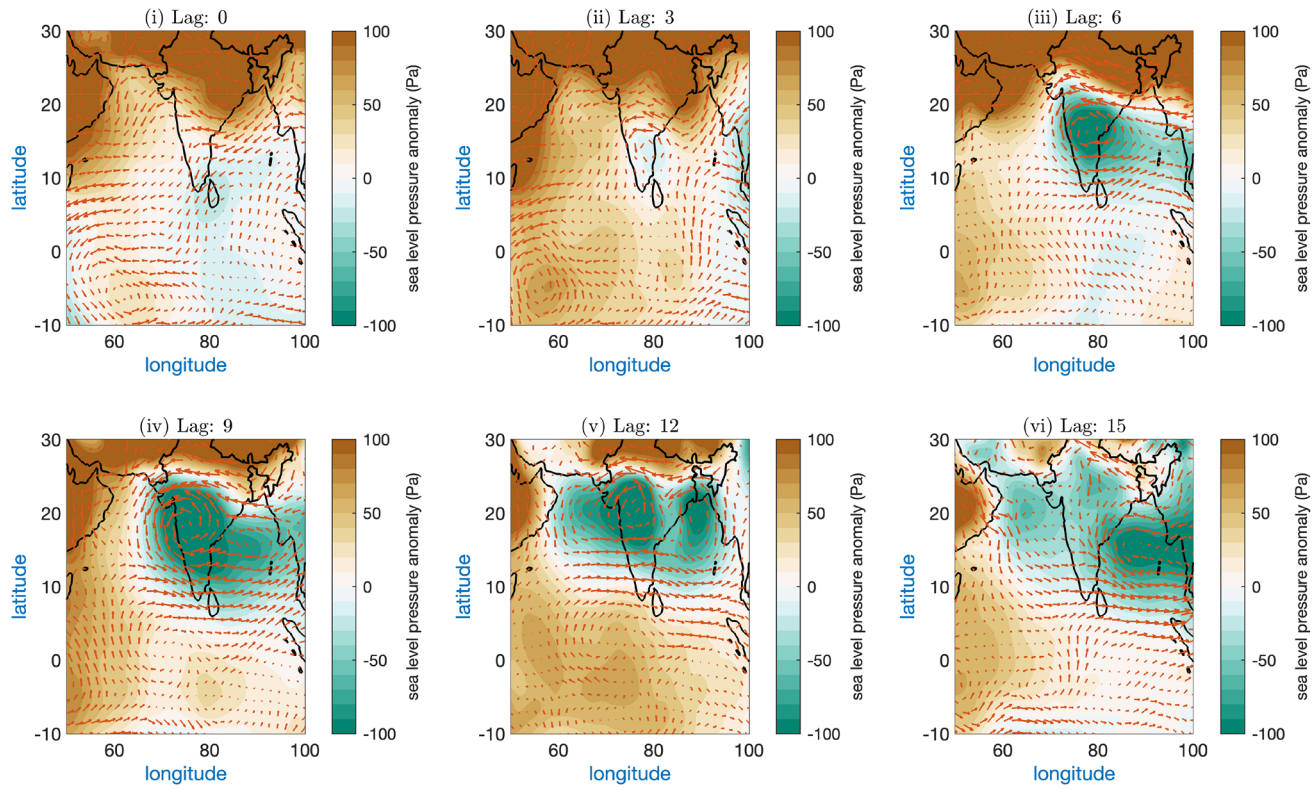


**Fig. 10** Propagation of the sea level pressure (SLP) from the (i) break condition (lag-0) to the (vi) active condition (lag-15) of MISO and the associated wind circulation at 850hPa in the RegCM4.7 simulation

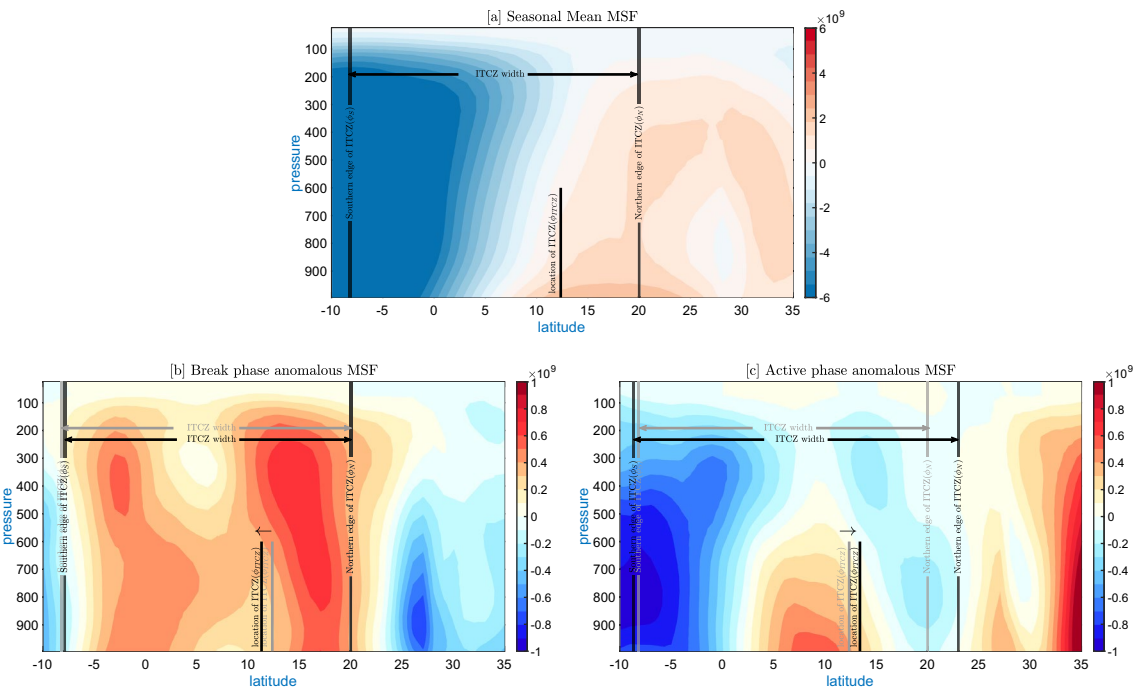


**Fig. 11** The regional component of the Hadley cell (RCHC) and ITCZ position and width for (a) summer (JJAS) seasonal mean conditions. Deviations of the RCHC and ITCZ position and width from the summer mean are shown for (b) MISO break phase and (c) MISO

active phase, identified from Fig. 4. The calculation of the RCHC and ITCZ positions and widths are explained in the text. The mean (MISO phase) ITCZ position and width is identified as black (grey) lines and arrows

phase, the main part of the RCHC is positioned closer to the equator. The high-pressure zone over the northern tropical region (Fig. 11b) is associated with this equatorial shift in the Hadley circulation during the break conditions over the Indian subcontinent. During the active phase, the low pressure over the Indian region and the northern tropic (Fig. 11c) is associated with northward shifts of the monsoonal RCHC. The results for the RCHC are generally consistent with those found for the SLP changes in the previous section.

### 3.5.3 ITCZ location and width

As a final link between background climate conditions and MISO development, we investigated links between the positioning and width of the model ITCZ during MISO phases. A previous study by Hari et al. (2020) shows that the northward propagation of the ITCZ region is linked with rainfall strength over India. The position of the ITCZ indeed shifts northward in the model during the active MISO phase and the ITCZ width expands on its northward side over southern India (Fig. 11c). The position of the ITCZ shifts southward in the model during the break phase while the ITCZ width expands slightly on the southern side (Fig. 11b). These changes in the model ITCZ width and position are associated with the strengthening and northward shifting in the RCHC over India during the active phase of MISO. This northward movement of the ITCZ over the Indian monsoon region, therefore, provides favorable conditions for the active part of MISO to propagate northwards. The reverse situation prevails during the model break periods. The results of this ITCZ analysis are consistent with the observational analysis of Hari et al. (2020) and the previous sections relating SLP and RCHC to the model MISO phases.

## 4 Summary and conclusions

We have analyzed a regional atmosphere model, freely evolving from 1979–2016 while forced by observed remote boundary conditions and local SST, for its ability produce northward propagating monsoon intraseasonal oscillations (MISO). The model, which is the latest version of RegCM4 run at 25 km resolution, produces organized northward propagating precipitation anomalies in the 25–90 day period band, with a dominant MISO period of 30 days (Figs. 6, 8) and a propagation speed of 1 deg/day (Fig. 7). The model MISO (Figs. 5c, d, 6, 8) broadly resembles the observations (Fig. 5c, d), but model precipitation bands are rotated slightly clockwise. The model MISO rainfall patterns are then linked to large-scale atmospheric model variables, with low SLP anomalies over India and the BoB favoring active phases of MISO. The low SLP patterns are then linked to

northward shifts over India of both the regional component of the Hadley Cell (RCHC) and ITCZ position and width (Fig. 11).

We also found that the total simulated seasonal (JJAS) mean rainfall anomalies over India are not significantly correlated with observations (Fig. 2), indicating that intrinsic variations in the regional model atmosphere dominate most of the precipitation variability aggregated over daily to seasonal time-scales. But we surprisingly found that a significant fraction of the model MISO are correlated (0.61) to observations (Fig. 4) when bandpassed to the 25–90 day period band. Since the model is remotely forced by atmospheric observations (EIN75) at very distant boundaries, this suggests some aspects of the large-scale circulation or the local SST anomaly must be causing the initiation of at least some of the model MISO events. This hypothesis needs to be tested in future simulations that can compare the results with runs where the local SST anomaly is set to zero and runs with the remote atmospheric boundary conditions set to climatology. Additionally, an ensemble of runs should run for the control case and for the experimental cases in order to quantify the level of intrinsic variability in MISO generation in the model compared to the boundary-forced part of the MISO initiation.

RegCM has been frequently used to study the Indian monsoon, but very little attention has been given to investigating the MISO of the Indian summer monsoon or their predictability. This study shows that predictable components of MISO clearly arise in the model system and suggests that forecasting experiments for MISO with specified initial conditions in RegCM4.7 may be fruitful for quantifying the level of skill. On another positive note, the structure of the statistical distributions of daily rainfall anomalies in key regions of the domain are quite similar with observations (Fig. 3). However, we also identified serious model biases in mean seasonal rainfall (Fig. 1) and the magnitude of MISO-related precipitation anomalies along the western coast of India (Fig. 5) that need to be ameliorated before making convincing progress in regional MISO modeling with RegCM4.7. The results of this study may help in targeting such attempts for model improvements in both uncoupled atmosphere and coupled atmosphere–ocean mode.

**Acknowledgements** This work forms a part of the Ph.D. dissertation of SG and was supported by a Fulbright Fellowship (2019 Fulbright-Kalam Climate Fellowships for Doctoral Research funded by USIEF and DST). We thank Matlab (v: 2019, 2020, 2021) and NCL (v: 6.6.2) for providing the visual platform for data handling, data analysis and data visualization. Analysis was carried out at the Cheyenne supercomputer (doi:10.5065/D6RX99HX) provided by NCAR’s Computational and Information Systems Laboratory (CISL). SG, ACS, and AJM are grateful for support by the United States Office of Naval Research MISO-BOB Departmental Research Initiative under grant N00014-17-1-2865. AJM was also partly supported by the National Science Foundation (OCE-2022868). SG acknowledge to Prof. William J. Gutowski for providing some critical feedback on the regional climate modeling. Authors are thankful to the ICTP and Goddard Earth Sciences Data and

Information Services Center (GES DISC) for the RegCM4.7 model and the TRMM rainfall data respectively.

**Funding** This study is supported by the 2019 Fulbright-Kalam Climate Fellowships for Doctoral Research funded by USIEF and DST. SG, ACS, and AJM are grateful for support by the United States Office of Naval Research MISO-BOB Departmental Research Initiative under grant N00014-17-1-2865. AJM was also partly supported by the National Science Foundation (OCE-2022868).

**Data availability** Enquiries about data availability should be directed to the authors.

## Declarations

**Conflict of interest** The authors have not disclosed any competing interests.

## References

- Abatan AA, Collins M, Babel MS et al (2021) Assessment of the ability of cmip6 gcms to simulate the boreal summer intraseasonal oscillation over southeast Asia. *Front Clim* 3:716129
- Abhik S, Mukhopadhyay P, Krishna R et al (2016) Diagnosis of boreal summer intraseasonal oscillation in high resolution ncep climate forecast system. *Clim Dyn* 46(9):3287–3303
- Abhilash S, Sahai A, Borah N et al (2014a) Prediction and monitoring of monsoon intraseasonal oscillations over Indian monsoon region in an ensemble prediction system using cfsv2. *Clim Dyn* 42(9):2801–2815
- Abhilash S, Sahai A, Pattnaik S et al (2014b) Extended range prediction of active-break spells of Indian summer monsoon rainfall using an ensemble prediction system in ncep climate forecast system. *Int J Climatol* 34(1):98–113
- Acharya N, Chattopadhyay S, Mohanty U et al (2013) On the bias correction of general circulation model output for Indian summer monsoon. *Meteorol Appl* 20(3):349–356
- Agrawal N, Singh BB, Pandey VK (2021) Fidelity of regional climate model v4.6 in capturing seasonal and subseasonal variability of Indian summer monsoon. *Dyn Atmos Oceans* 94(101):203
- Annamalai H, Slingo J (2001) Active/break cycles: diagnosis of the intraseasonal variability of the Asian summer monsoon. *Clim Dyn* 18(1):85–102
- Bhatla R, Ghosh S, Mandal B et al (2016) Simulation of Indian summer monsoon onset with different parameterization convection schemes of REGCM-4.3. *Atmos Res* 176:10–18
- Byrne MP, Pendergrass AG, Rapp AD et al (2018) Response of the intertropical convergence zone to climate change: location, width, and strength. *Curr Clim Change Rep* 4(4):355–370
- Chen X, Pauluis OM, Zhang F (2018) Regional simulation of Indian summer monsoon intraseasonal oscillations at gray-zone resolution. *Atmos Chem Phys* 18(2):1003–1022
- Dee DP, Uppala SM, Simmons AJ et al (2011) The era-interim reanalysis: configuration and performance of the data assimilation system. *Q J R Meteorol Soc* 137(656):553–597
- Elguindi N, Bi X, Giorgi F, et al (2013) Regional climate model regcm user manual version 4.4. The Abdus Salam International Centre for Theoretical Physics, Strada Costiera, Trieste, Italy October 21(2013):54
- Emanuel KA, Živković-Rothman M (1999) Development and evaluation of a convection scheme for use in climate models. *J Atmos Sci* 56(11):1766–1782
- Fang Y, Wu P, Mizielski M et al (2017) Monsoon intra-seasonal variability in a high-resolution version of met office global coupled model. *Tellus A Dyn Meteorol Oceanogr* 69(1):1354661
- Fu X, Wang B, Waliser DE et al (2007) Impact of atmosphere–ocean coupling on the predictability of monsoon intraseasonal oscillations. *J Atmos Sci* 64(1):157–174
- Fu X, Lee JY, Wang B et al (2013) Intraseasonal forecasting of the Asian summer monsoon in four operational and research models. *J Clim* 26(12):4186–4203
- Ghosh S (2020) Climate modeling and simulation of indian summer monsoon dynamics. Ph.D. Dissertation, BHU: Varanasi, India
- Ghosh S, Bhatla R, Mall R et al (2019) Aspect of ECMWF downscaled regional climate modeling in simulating Indian summer monsoon rainfall and dependencies on lateral boundary conditions. *Theor Appl Climatol* 135(3):1559–1581
- Ghosh S, Sinha P, Bhatla R et al (2022) Assessment of lead-lag and spatial changes in simulating different epochs of the Indian summer monsoon using regcm4. *Atmos Res* 265(105):892
- Giorgi F, Coppola E, Solmon F et al (2012) Regcm4: model description and preliminary tests over multiple cordex domains. *Clim Res* 52:7–29
- Goswami B (2005) South Asian monsoon. In: *Intraseasonal variability in the atmosphere–ocean climate system*, wkm lau and de waliser, eds. Praxis pp 19–61
- Grell GA, Dudhia J, Stauffer DR, et al (1994) A description of the fifth-generation penn state/ncar mesoscale model (mm5)
- Grenier H, Bretherton CS (2001) A moist pbl parameterization for large-scale models and its application to subtropical cloud-topped marine boundary layers. *Mon Weather Rev* 129(3):357–377
- Gutowski WJ Jr, Giorgi F, Timbal B et al (2016) Wcrp coordinated regional downscaling experiment (cordex): a diagnostic mip for cmip6. *Geosci Model Dev* 9(11):4087–4095
- Hari V, Villarini G, Karmakar S et al (2020) Northward propagation of the intertropical convergence zone and strengthening of Indian summer monsoon rainfall. *Geophys Res Lett* 47(23):e2020GL089823
- Huffman GJ, Bolvin DT (2018) Real-time trmm multi-satellite precipitation analysis data set documentation. NASA Tech Doc 10
- Kiehl J, Hack J, Bonan G, et al (1996) Description of the ncar community climate model (ccm3). Technical note. Tech. rep., National Center for Atmospheric Research, Boulder, CO (United States)
- Kikuchi K, Wang B, Kajikawa Y (2012) Bimodal representation of the tropical intraseasonal oscillation. *Clim Dyn* 38(9):1989–2000
- Lau WKM, Waliser DE (2011) Intraseasonal variability in the atmosphere–ocean climate system. Springer Science & Business Media, Berlin
- Lee JY, Wang B, Wheeler MC et al (2013) Real-time multivariate indices for the boreal summer intraseasonal oscillation over the Asian summer monsoon region. *Clim Dyn* 40(1):493–509
- Lee SS, Wang B, Waliser DE et al (2015) Predictability and prediction skill of the boreal summer intraseasonal oscillation in the intraseasonal variability hindcast experiment. *Clim Dyn* 45(7):2123–2135
- Li Y, Han W, Wang W et al (2018) The Indian summer monsoon intraseasonal oscillations in cfsv2 forecasts: biases and importance of improving air–sea interaction processes. *J Clim* 31(14):5351–5370
- Li B, Chen D, Lian T et al (2022a) Comparison of coupled and uncoupled models in simulating monsoon intraseasonal oscillation from cmip6. *Acta Oceanol Sin* 41(10):100–108
- Li B, Zhou L, Qin J et al (2022b) Key process diagnostics for monsoon intraseasonal oscillation over the Indian ocean in coupled cmip6 models. *Clim Dyn* 59(9–10):2853–2870
- Maharana P, Dimri A (2016) Study of intraseasonal variability of Indian summer monsoon using a regional climate model. *Clim Dyn* 46(3):1043–1064

- Misra V, Mishra A, Bhardwaj A (2018) Simulation of the intraseasonal variations of the Indian summer monsoon in a regional coupled ocean–atmosphere model. *J Clim* 31(8):3167–3185
- Mooley D, Shukla J (1989) Main features of the westward-moving low pressure systems which form over the Indian region during the summer monsoon season and their relation to the monsoon rainfall. *Mausam* 40(2):35–50
- North GR, Bell TL, Cahalan RF et al (1982) Sampling errors in the estimation of empirical orthogonal functions. *Mon Weather Rev* 110(7):699–706
- Oleson K, Lawrence D, Bonan G, et al (2013) Technical description of version 4.5 of the community land model (clm) (no. ncar/tm-503+str). UCAR, Boulder, CO, USA
- Pal JS, Small EE, Eltahir EA (2000) Simulation of regional-scale water and energy budgets: representation of subgrid cloud and precipitation processes within REGCM. *J Geophys Res Atmos* 105(D24):29579–29594
- Rao Y (1976) Southwest monsoon (meteorological monograph, synoptic meteorology no. 1). Indian Meteorological Department, New Delhi 367
- Sabeerali C, Ramu Dandi A, Dhakate A et al (2013) Simulation of boreal summer intraseasonal oscillations in the latest cmip5 coupled GCMS. *J Geophys Res Atmos* 118(10):4401–4420
- Shahi NK, Das S, Ghosh S et al (2021) Projected changes in the mean and intra-seasonal variability of the Indian summer monsoon in the REGCM cordex-core simulations under higher warming conditions. *Clim Dyn* 57(5):1489–1506
- Sikka D, Gadgil S (1980) On the maximum cloud zone and the ITCZ over Indian longitudes during the southwest monsoon. *Mon Weather Rev* 108(11):1840–1853
- Sperber KR, Annamalai H (2008) Coupled model simulations of boreal summer intraseasonal (30–50 day) variability, part 1: systematic errors and caution on use of metrics. *Clim Dyn* 31(2):345–372
- Sperber K, Annamalai H, Kang IS et al (2013) The Asian summer monsoon: an intercomparison of cmip5 vs cmip3 simulations of the late 20th century. *Clim Dyn* 41(9):2711–2744
- Suhas E, Neena J, Goswami B (2013) An Indian monsoon intraseasonal oscillations (miso) index for real time monitoring and forecast verification. *Clim Dyn* 40(11):2605–2616
- Tiedtke M (1989) A comprehensive mass flux scheme for cumulus parameterization in large-scale models. *Mon Weather Rev* 117(8):1779–1800
- Vitart F (2014) Evolution of ECMWF sub-seasonal forecast skill scores. *Q J R Meteorol Soc* 140(683):1889–1899
- Vitart F, Robertson AW, Anderson DL (2012) Subseasonal to seasonal prediction project: bridging the gap between weather and climate. *Bull World Meteorol Organ* 61(2):23
- Waliser D, Stern W, Schubert S et al (2003) Dynamic predictability of intraseasonal variability associated with the Asian summer monsoon. *Q J R Meteorol Soc J Atmos Sci Appl Meteorol Phys Oceanogr* 129(594):2897–2925
- Weare BC, Nasstrom JS (1982) Examples of extended empirical orthogonal function analyses. *Mon Weather Rev* 110(6):481–485
- Webster PJ, Magaña VO, Palmer T et al (1998) Monsoons: processes, predictability, and the prospects for prediction. *J Geophys Res Oceans* 103(C7):14,451–14,510
- Zeng X, Zhao M, Dickinson RE (1998) Intercomparison of bulk aerodynamic algorithms for the computation of sea surface fluxes using toga coare and tao data. *J Clim* 11(10):2628–2644

**Publisher's Note** Springer Nature remains neutral with regard to jurisdictional claims in published maps and institutional affiliations.

Springer Nature or its licensor (e.g. a society or other partner) holds exclusive rights to this article under a publishing agreement with the author(s) or other rightsholder(s); author self-archiving of the accepted manuscript version of this article is solely governed by the terms of such publishing agreement and applicable law.